

LIBRARY Michigan State University

This is to certify that the thesis entitled

Analytical and Experimental Modal Synthesis

presented by

James Herman Oliver

has been accepted towards fulfillment of the requirements for

M.S.

_degree in _

Mech. Engr.

Major professor

te 2 | 76 | 8 |

O-7639



OVERDUE FINES: 25¢ per day per item

RETURNING LIBRARY MATERIALS: Place in book return to remove charge from circulation records

SEP 2 8 2004

ANALYTICAL AND EXPERIMENTAL MODAL SYNTHESIS

by

James Herman Oliver

A THESIS

Submitted to
Michigan State University
in partial fulfillment of the requirements
for the degree of

MASTER OF SCIENCE

Department of Mechanical Engineering

ABSTRACT

ANALYTICAL AND EXPERIMENTAL MODAL SYNTHESIS

Ву

James Herman Oliver

This thesis presents modal analysis of an automotive flywheel using both analytical and experimental techniques. The analytical work was performed with the finite element code ANSYS, and the experimental work was performed with the GenRad 2507 Structural Analysis System. Each technique was used to determine natural frequencies and mode shapes of the flywheel. Correlation of the results serves as the basis for a discussion of the effects of modelling approximations.

ACKNOWLEDGEMENTS

I would like to express my sincere gratitude to Dr. James E. Bernard, my major professor. His advice in both academic and personal matters has proved extremely valuable for my career goals.

Also, many thanks to Dr. C.J. Radcliffe and Dr. R.C. Rosenberg whose comments and advice on this thesis were greatly appreciated.

A special thanks to all six of my sisters for their enthusiastic support. I would particularly like to thank my sister Linda and her husband, Gene Allen, whose generosity and hospitality helped make my transition to graduate life quite enjoyable. And, of course, the loving support of my parents, Vince and Caroll Oliver, has always inspired me to do my best.

Finally, thanks to all my friends at MSU and in East Lansing for helping make my graduate career a truly great experience.

TABLE OF CONTENTS

LIST OF	TABLES.	iv
LIST OF	FIGURES	Sv
Chapter	1 -	INTRODUCTION1
Chapter	2 -	THE FLYWHEEL2
Chapter	3 -	MODAL TESTING4
Chapter	3.1 3.2 3.3 3.4 3.5 3.6 3.7 4 - 4.1 4.2 4.3 4.4 4.5	Test Equipment and Setup
Chapter		4.5.1 Counterweight
Chapter		CONCLUSIONS
•		NCES

LIST OF TABLES

3.1	Test Conditions10
3.2	Modal Parameters20
4.1	Effects of the Refined Element Mesh39
4.2	Counterweight Analysis43
4.3	Effects of the Number of Master Degrees of Freedom43
4.4	Effects of Material Property Modification45
4.5	Analytical and Experimental Results54

LIST OF FIGURES

2-1	The Flywheel3
3-1	Impact Testing Method5
3-2	Test Setup
3-3	Flywheel with Node Locations8
3-4	Undeformed Geometry10
3-5	Input and Output Signals13
3-6	Power Spectrum of Input Signal14
3-7	Coherence Function17
3 - 8	Frequency Response Function17
3-9	Multi Degree of Freedom Curve Fit
3-10	Single Degree of Freedom Circle Fits22
3-11	Mode Shape at First Natural Frequency (Experimental)24
3-12	Synthesized Frequency Response Function24
4-1	Element Mesh34
4-2	Mode Shape at First Natural Frequency (Finite Element Method)
4-3	Refined Element Mesh38
4-4	Element Mesh with Counterweight Location Denoted by Shading40
5-1	First Mode Shape - Experimental47
5-2	Second Mode Shape - Experimental47
5-3	Third Mode Shape - Experimental48

5-4	Fourth Mode Shape - Experimental	48
5-5	Fifth Mode Shape - Experimental	49
5-6	Sixth Mode Shape - Experimental	49
5-7	First Mode Shape - Finite Element Method	50
5-8	Second Mode Shape - Finite Element Method	50
5-9	Third Mode Shape - Finite Element Method	51
5-10	Fourth Mode Shape - Finite Element Method	51
5-11	Fifth Mode Shape - Finite Element Method	52
5-12	Sixth Mode Shape - Finite Flement Method	52

INTRODUCTION

Modal analysis characterizes the dynamics of a structure by identifying its modes of vibration. Each mode consists of a resonant frequency, a damping ratio and a mode shape defining the displacement of the structure at each resonant frequency. The modes of vibration may be considered properties of the structure.

In recent years, the finite element method has become an increasingly popular tool for the study of structural dynamics. To gain confidence in finite element results it is expedient to check the validity of the mathematical model. Traditionally this has been done by making rough approximations through "hand" solutions on a simplified model, or by other analytical techniques which bound the eigenvalues. However, if the structure is available, modal testing via digital signal processing offers an independent verification.

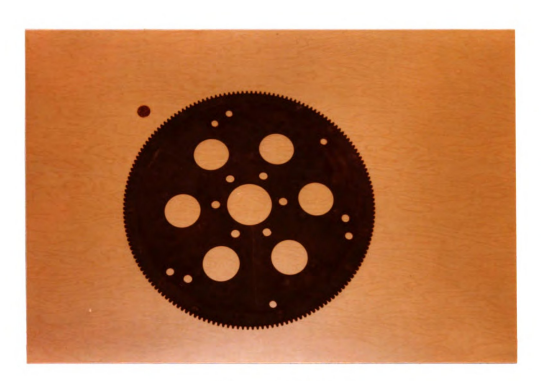
This thesis will discuss an application of both finite element and experimental techniques for performing modal analysis on a simple structure. Chapter 2 describes the structure under consideration, an automotive flywheel. Chapter 3 discusses modal testing, and Chapter 4 deals with modal analysis using the finite element method. Chapter 5 presents correlation of results obtained by the two methods. Conclusions are presented in Chapter 6.

THE FLYWHEEL

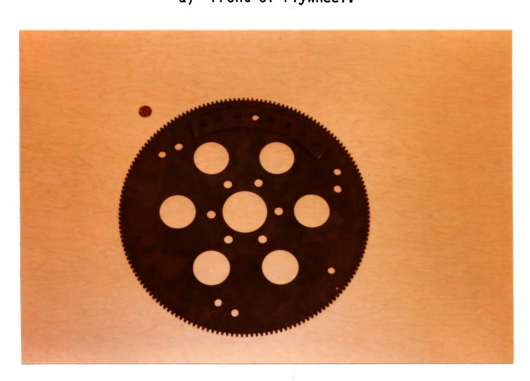
The structure addressed in this study is a standard automotive flywheel from a General Motors 350 CID engine. The flywheel was obtained from an auto salvage yard. It was then sandblasted to remove oxidation.

Figure 2-1 shows both sides of the flywheel. The mean diameter of the flywheel is approximately 13.75 inches. The center hole is 2.5 inches in diameter. This is surrounded by six equally spaced mounting holes, each approximately 1/2 inch in diameter. The six large circumferential holes are each 2 inches in diameter.

The interior part of the disk has apparently been stamped from 0.112 inch thick sheet steel. (Thickness was measured after sandblasting.) The outer gear ring, approximately 0.371 inches thick, was probably cast. These pieces are attached with twelve equally spaced circumferential welds, each of which is about 1.35 inches long. A counterweight is attached to the back of the flywheel, near the intersection of the interior plate and the gear ring. See Figure 2-lb. The counterweight spans an arc of approximately 85° and is attached to the flywheel with several small welds.



a) Front of Flywheel.



b) Back of Flywheel.

Figure 2-1 The Flywheel.

MODAL TESTING

Modal testing is a means of characterizing the dynamic behavior of a structure. Specifically, by exciting the structure with applied forces, its natural frequencies, mode shapes, and modal damping values can be identified. Since these parameters are derived experimentally, modal testing provides an independent verification for analytical solution techniques such as the finite element method.

This chapter will develop the procedure used in the impact method of modal testing. Figure 3-1 [11] presents a schematic diagram of the impact testing method. The structure is subjected to an impulse force at one point and the acceleration response is measured at another point. The pair of input-output signals is then processed with a Fast Fourier Transform (FFT) algorithm. The resulting ratio, output acceleration over input force, forms the frequency response function relating that pair of points.

A data base of frequency response functions is created relating several driven points to a reference point. Curve fitting algorithms are then applied to the data base to determine the modal parameters: natural frequencies, mode shapes, and modal damping values.

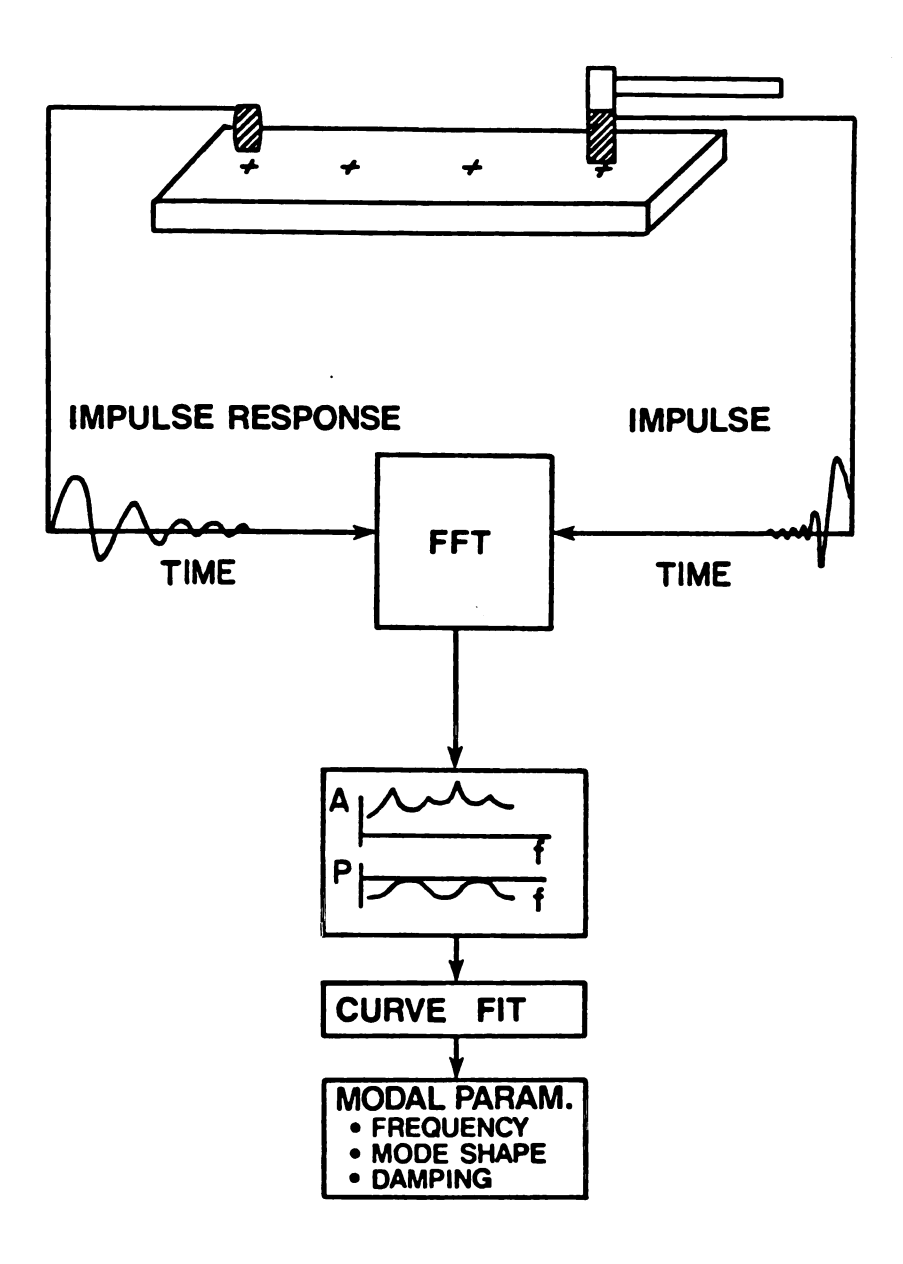


Figure 3.1 Impact Testing Method.

This procedure was applied to obtain modal parameters for the flywheel. A detailed discussion of each step of the procedure will be presented in the following sequence:

Test Equipment and Setup

Geometry Definition

Specification of Test Conditions

Data Acquisition

Modal Parameter Extraction

Mode Shape Calculation

Validity of Modal Data Base

3.1 Test Equipment and Setup

The GenRad 2507 Structural Analysis System was used to perform the modal testing. This device incorporates the SDRC MODAL PLUS software package. MODAL PLUS is a product of Structural Dynamics Research Corporation (SDRC) of Cincinnati, Ohio. The GenRad 2507 is made by GenRad Inc. of Santa Clara, California. The major components of the GenRad 2507 include; a PDP 11/04 minicomputer-controller; a high speed micro-programmed processor for Fast Fourier Transform; a dual floppy disk drive; an analog to digital converter; a raster-scan type video graphic display terminal; and a hard copy printer/plotter.

Other necessary equipment are the impact force hammer, response accelerometer, and accompanying amplifiers and cables. These devices were made by PCB Piezotronics Inc. The impact hammer is equipped with a force transducer in the tip to measure input force. The

accelerometer and transducer are each connected to a separate amplifier. These, in turn, are connected to two separate channels on the A/D converter of the GenRad; input force on channel A, output acceleration on channel B.

To simulate free-free boundary conditions, the flywheel was tested while resting upon a 4 inch thick foam rubber cushion. A rigid body mode of the flywheel on the cushion was, therefore, expected.

Figure 3-2 shows the complete experimental setup prepared for a test.

3.2 Geometry Definition

The geometry of the structure must be defined to allow graphical presentation of the mode shapes. This was accomplished by selecting a coordinate system and defining the coordinates of a number of points on the structure. A sufficient number of points must be selected to facilitate observation of the highest frequency modes of interest, i.e., enough to visualize a complicated distortion of the structure. But, although additional points improve the visualization of the mode shape, each additional point requires additional data collection and storage.

In this case, 48 points were used to describe the flywheel. Figure 3-3 shows the flywheel these locations identified. The coordinate of each points was input into the MODAL PLUS program. The geometry was then previewed to insure proper point location and connectivity. Figure 3-4, output of MODAL PLUS, shows the geometry in an undeformed shape. Note, in Figure 3-4, a chord



Figure 3-2 Test Setup.

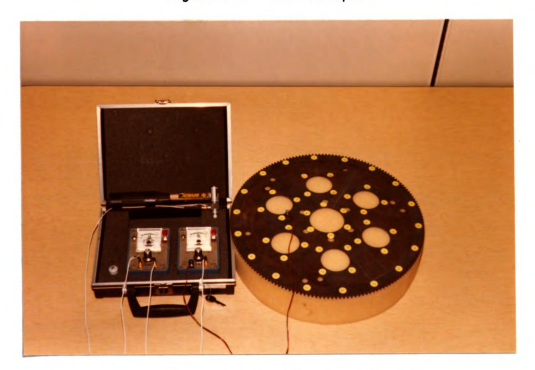


Figure 3-3 Flywheel with Node Locations.

connecting two points on the circumference. This represents the approximate location of the counterweight mounted on the back of the flywheel.

At this point in the procedure a reference coordinate must be selected. The reference coordinate is the position on the structure where response to the input forces is measured. The position must be selected such that there is sufficient amplitude for all modes of interest. No response could be measured if the reference coordinate corresponded to a nodal point (or line) for a particular mode.

In this case, the decision for the location was based on advance knowledge of the first few mode shapes [1]. Based on this information the accelerometer was located on the interior section of the flywheel, at point number 10. (See Figure 3-4.) Proper selection of the reference coordinate was confirmed later by the finite element analysis.

3.3 Specification of Test Conditions

Test conditions are required input for MODAL PLUS to calibrate the system and prepare it for data acquisition. Table 3.1 (output of MODAL PLUS) lists the test conditions used for this modal test.

Many of the test conditions are determined with the aid of MODAL PLUS. However, some of the conditions listed in Table 3.1 do not apply to a two channel system, some are not used in the current version of MODAL PLUS, and some are set automatically based on selection of other conditions. The following discussion considers the significant test conditions.

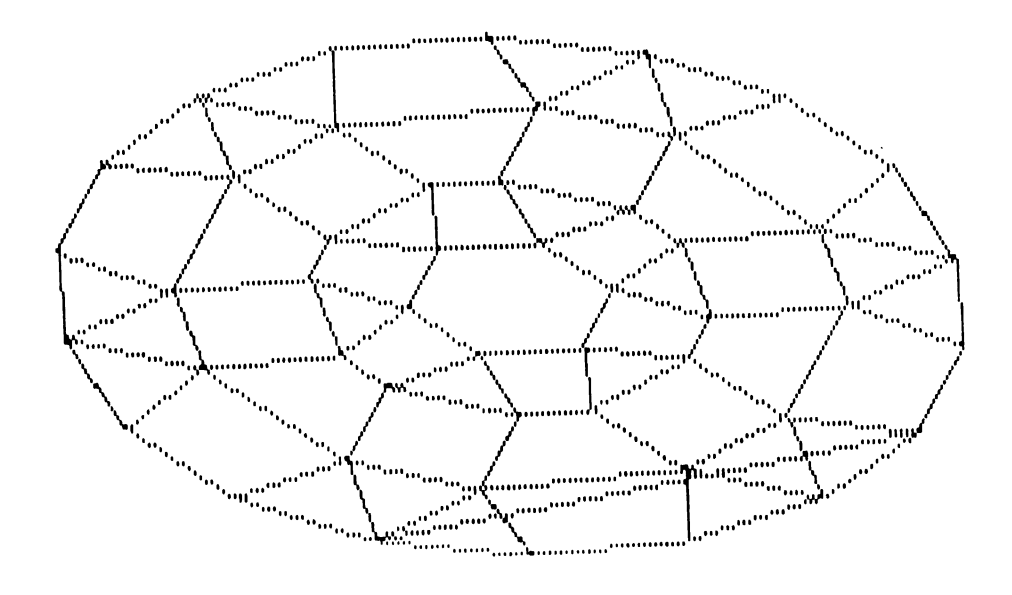


Figure 3.4 Undeformed Geometry.

TABLE 3.1

Test Conditions

1234567890112314519	TRIGGER TYPE TRIGGER LEVEL COUPLING CODE HANNING CODE ENSEMBLE SIZE MAXIMUM FREQ A-A FILTERS EXCITATION FREGRESP 1 FREGRESP 2 FREGRESP 3 OVERRANGES CLEAR FREQ L CLEAR FREQ U MINIMUM FREQ MASTER IDENT	1 10 9 9 5 1000.0 1000.0 1 21 0 0 0 0.00000 1000.0 0.00000	20 AUXIL 21 CH 01 22 CH 02 23 CH 03 24 CH 04 25 CH 01 26 CH 02 27 CH 03 28 CH 04 29 CH 01 30 CH 02 31 CH 03 32 CH 04	RANGE RANGE RANGE RANGE SCALE SCALE SCALE SIGNAL SIGNAL SIGNAL	1.0000 0.50000 1.0000 1.0000 1.0000 1.00000 0.00000 0.00000 4 33 33
			** FLYWH	L MODAL **	

The impact method of excitation was chosen because it is fast, easy to perform and requires less equipment and setup time than random methods (which require use of a shaker). The maximum frequency was decided upon based on preliminary calculations [1] to determine natural frequencies of a uniform circular plate. The frequency range 0-1000 Hz was judged sufficient to observe several modes of vibration.

The first condition in Table 3.1, trigger type, set to 1, indicates impact excitation with internal trigger. The term "trigger" refers to when the time sample of the signals will be taken. A positive value for trigger type indicates triggering on the positive slope of the input (force) signal. Trigger level (item 2, Table 3.1) is the percentage of full scale voltage necessary to trigger time sampling.

The ensemble size (item 5) is the number of time samples averaged to calculate a frequency response function. A large number of samples reduces the effect of noise in the calculated function. In this case 5 samples at each measurement point were taken. The relation between ensemble size and data quality, the coherence function, will be examined in Section 3.4.

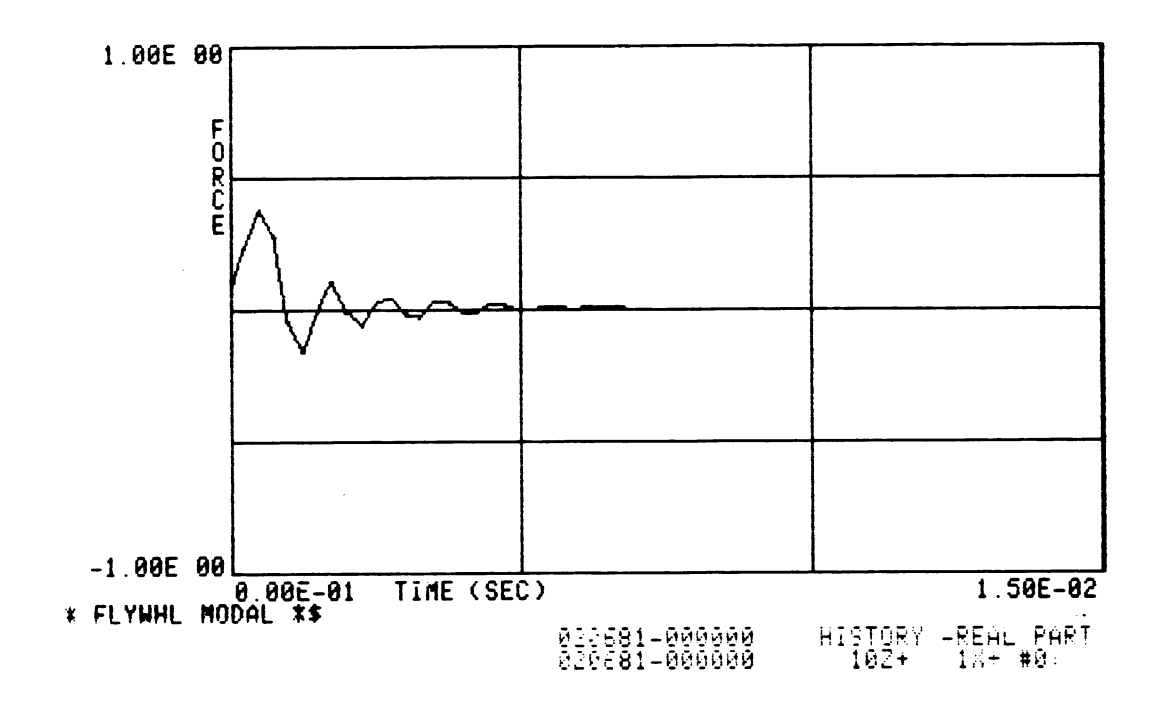
Specification of maximum frequency (item 6) at 1000 Hz automatically sets conditions 7, 13, and 14. Condition 7 specifies the cut off frequency for the anti-aliasing filter. Aliasing is a form of amplitude distortion introduced by sampling a continuous signal at discrete times. Specifically, if the sampling rate is not greater than twice the highest frequency of any component in the signal (Nyquist frequency), then some of the signal's high

frequency components will be effectively translated down in frequency when the FFT is applied. This unacceptable contamination of the data is minimized by filtering out all components of the signal higher than the required maximum frequency. Conditions 13 and 14 are further signal conditioning parameters based on selection of the maximum frequency.

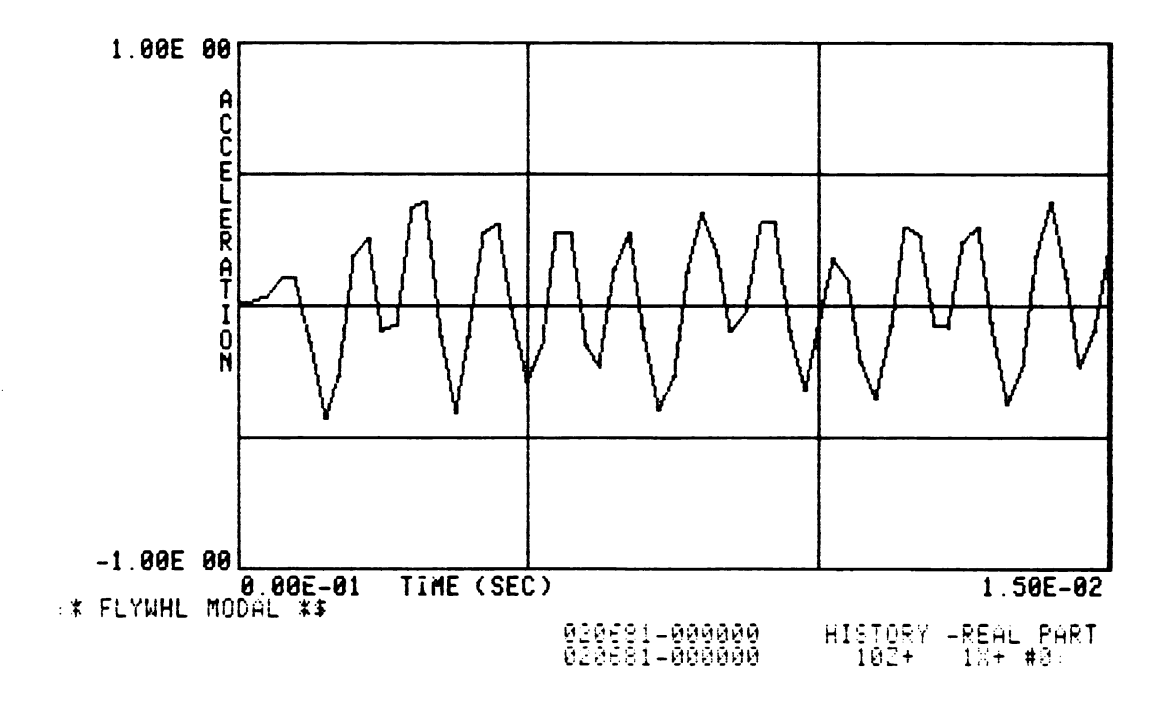
Items 25 and 26 in Table 3.1 are calibration factors. They represent the ratio of output units to input voltages. The values, given by the manufacturers, are 100 lbf/volt for the force transducer (channel A), and 100 g's/volt for the accelerometer (channel B). The amplifiers are equipped with a gain selector so that these values may be adjusted if necessary.

The remaining conditions are set by using the GenRad as an oscilloscope and observing some sample signals. Figure 3-5 shows a sample impact force and response acceleration time history. For best results, the maximum amplitude of the signals should be fifty to ninety percent of full range. Items 21 and 22 in Table 3.1, set to 0.5 and 1.0, specify the full scale voltage range for the force and acceleration signals, respectively. By adjusting input voltage range (item 21) and trigger level (item 2, Table 3.1), the magnitude of the impact necessary to trigger sampling can be adjusted to the users preference.

Finally, the power spectrum of the input signal must be examined to insure its frequency content is sufficient. Since objective of impact testing is to simultaneously excite all the modes of the structure within a specific frequency range, the input signal must have adequate energy content throughout that range.



a) Input Force Time History.



b) Output Acceleration Time History.

Figure 3-5 Input and Output Signals.

The frequency content of an impulse signal is inversely proportional to the duration of the initial pulse. The duration of the impulse depends on the hardness of the hammer tip. A softer tip imparts a longer duration signal than does a hard one. Therefore, a hard hammer tip can be used to emphasize higher frequency excitation whereas a softer tip would emphasize lower frequency excitation. Figure 3-6 shows the power spectrum of a sample force signal. In this case, a medium hardness (plastic) tip was used. The figure indicates that the signal has sufficient frequency content for the range 0 to 1000 Hz.

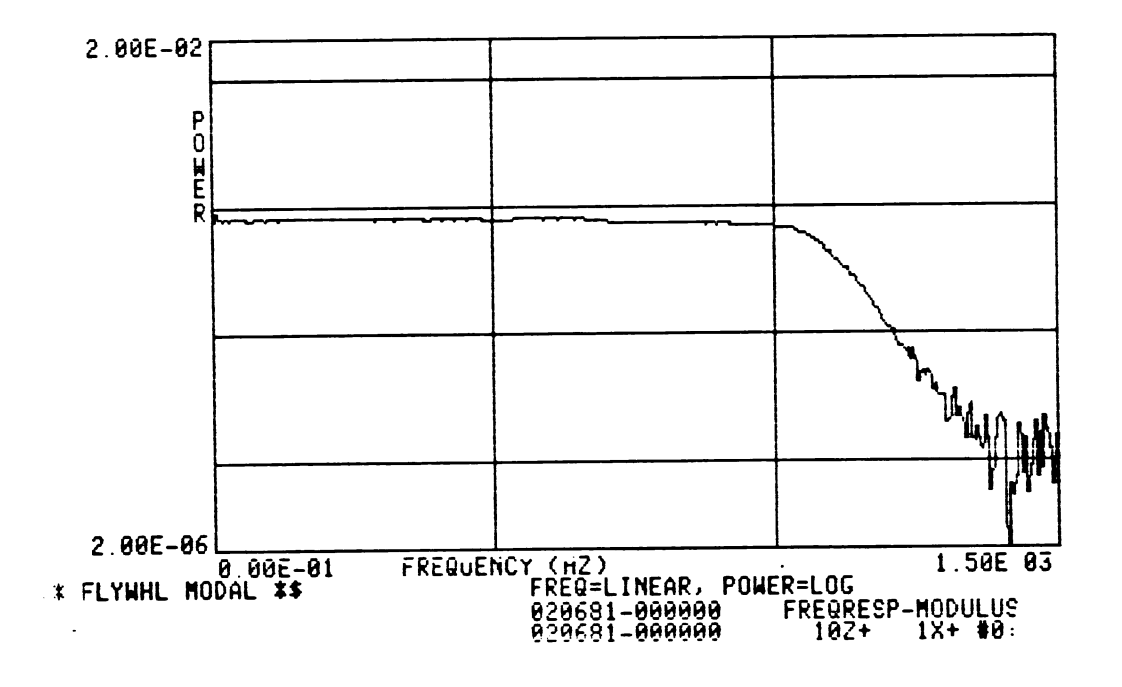


Figure 3-6 Power Spectrum of Input Signal.

3.4 Data Acquisition

The major concern during data acquisition is the quality of measured data. Since noise is always present in the measured signal, the user must determine to what degree the measured data has been contaminated. This is facilitated by the use of the coherence function.

The coherence function is the ratio of response power caused by applied input to measured response power. Thus, a perfect measurement, one with no noise contribution, would present a coherence equal to one throughout the frequency range. The coherence function is calculated in terms of averaged input and output auto-power and crosspower spectrums. Therefore, as the number of averages increases, the contribution of noise in the measurement decreases. Reference [2] provides a good discussion of the coherence function and computation of the transfer function in the presence of noise.

To acquire modal data, the flywheel was struck five times at each of the 48 points. In the process, care was taken to avoid rebound from the initial impact (i.e., a double hit), which is one of the easiest ways to introduce extraneous noise. In addition, if the hammer strike is too hard, the input signal overranges its set maximum value, and the sample is rejected. If the strike is too light, the input signal never reaches the trigger level and nothing happens. After five successful impacts, the coherence function was checked. If the coherence proved acceptable, the frequency response function was stored. The frequency response function (ratio of transformed output acceleration over transformed

input force) represents the measured modal data. The modal data base was complete when all 48 frequency response functions were stored.

Figure 3-7 shows a typical acceptable coherence function from the flywheel test. The frequency response function obtained from the data presented in Figure 3-8. The upper plot of Figure 3-8 shows the phase corresponding to the frequency response function.

3.5 Modal Parameter Extraction

Two methods are employed in MODAL PLUS for extracting modal parameters. To estimate natural frequencies and modal damping, a multi-degree of freedom (MDOF) curve fitting algorithm is used. Mode shapes are then calculated with a single-degree of freedom circle fitting algorithm. Mode shape calculation is discussed in the following section.

The MDOF curve fitting technique involves fitting a polynomial representation of the frequency response function to the measured data over a frequency range containing several resonance peaks. Figure 3-9 shows the polynomial form of the frequency response function and the resulting curve fit to a segment of measured data.

Peaks in the frequency response function represent areas of high amplitude magnification. Hence, they are referred to as resonant or natural frequencies. Before implementation of the MDOF curve fit, the various frequency response functions must be reviewed to find one which has a representative peak at all the suspected

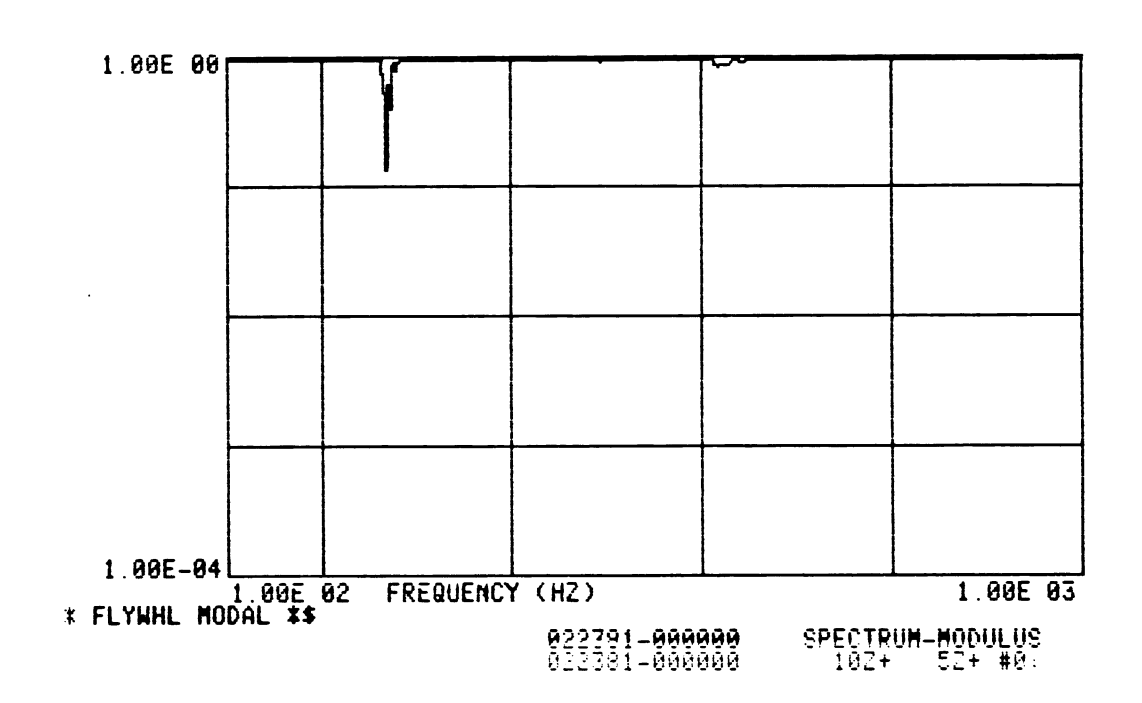


Figure 3-7 Coherence Function.

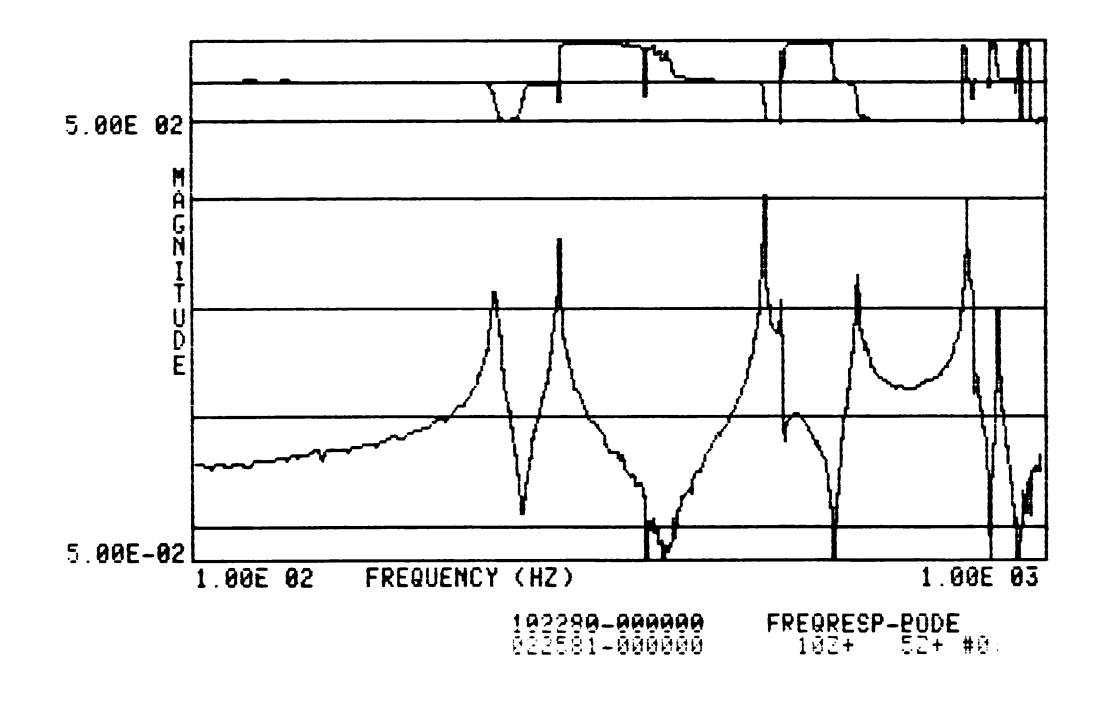


Figure 3-8 Frequency Response Function.

Polynomial Form:

$$H(s) = \frac{A_0 + A_1 s + A_2 s^2 + \dots + A_m s^m}{B_0 + B_1 s + B_2 s^2 + \dots + B_n s^n} \bigg|_{s = j\omega}$$

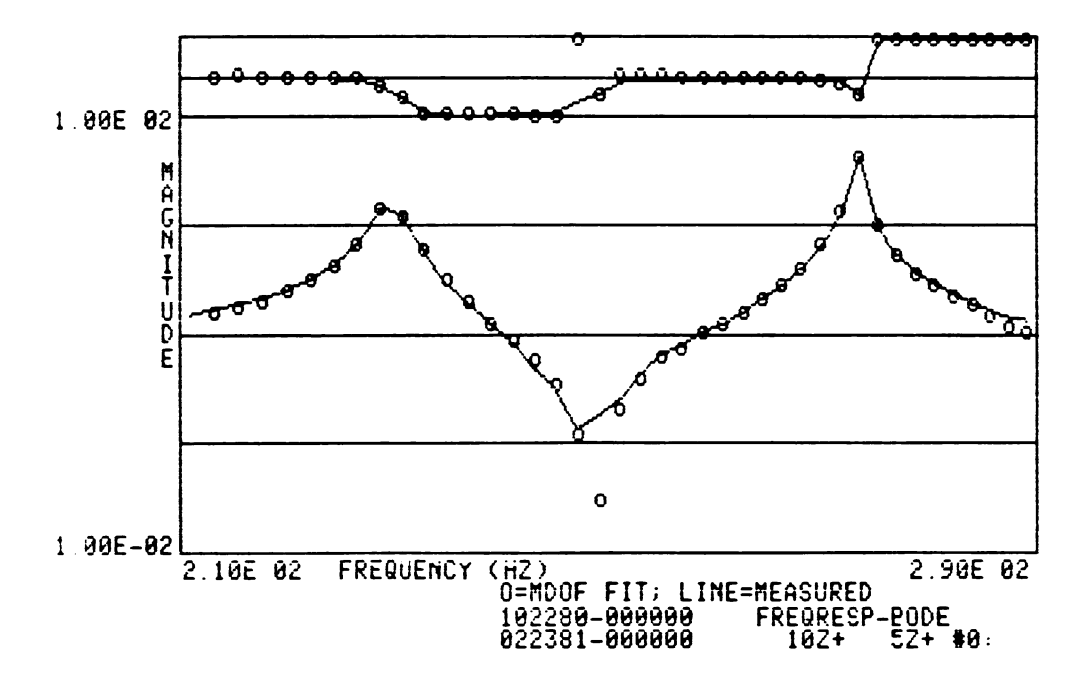


Figure 3-9 Multi Degree of Freedom Curve Fit.

natural frequencies. One point for example, could lie on or near a nodal point (or line) of a given mode. The frequency response function relating such a point to the reference point would show a small amplitude at that natural frequency. Figure 3-8 illustrates six peaks in the range 100-1000 Hz. Two small peaks at approximately 15 and 20 Hz were evidence of rigid body modes.

After a useful frequency response function is chosen a frequency band containing several resonant peaks must be selected. The approximate number of roots to be generated (i.e. the order of the polynomials in Figure 3-9) can then be chosen. The number of roots should be at least twice the number of apparent peaks in the selected frequency range but not more than eight times this number [3]. The roots of the approximating polynomial are extracted yielding, for each root, the modal parameters; frequency, damping ratio, amplitude and phase. From this list of data the natural frequencies are identified by those roots which present large amplitude with very little damping. If such a distinction is not obvious, the procedure must be repeated using a smaller frequency range and/or more roots. References [4] and [5] provide a detailed description of the MDOF curve fit technique.

Table 3.2 presents the modal parameters obtained in the flywheel test. In this case the frequency response function relating point 5 to the reference point 10 was used to extract all the modal parameters.

TABLE 3.2
Modal Parameters

LABEL	FREQ	DAMPING	AMPLITUDE	PHASE	REF	RES	MODE
1	227.128	0.004656	86.20	1.7227	10Z+	52+	1
2	271.818	0.000858	96.01	1.1678	10Z+	5Z+	2
3	470.844	0.000953	338.6	1.1759	10Z+	5Z+	3
4	604.367	0.005038	241.5	1.8504	10Z+	5Z+	4
5	812.012	0.001580	704.2	-1.6498	10Z+	5Z+	5
6	882.826	0.000969	49.49	-1.9259	10Z+	5Z+	6
#							

3.6 Mode Shape Calculation

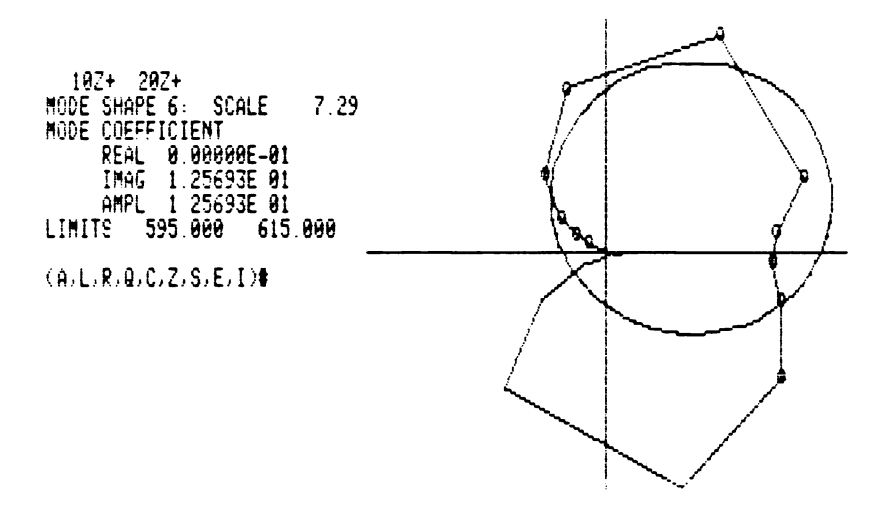
Mode shapes are approximated with a single-degree of freedom (SDOF) circle fitting algorithm. A SDOF system has one resonant frequency. A plot of the real versus imaginary parts of the frequency response function for such a system (as frequency varies through resonance) would form a perfect circle. This is commonly known as the Nyquist plot.

As applied in this case, the Nyquist plot for one peak would not form a circle because the frequency response function is a summation of the effects of all modes. However, if the modes are sufficiently spaced, and the frequency band about resonance is small enough, the resulting plot can be approximated by a circle. Since a measured frequency response function is composed of discrete spectral information, the Nyquist plot appears as several data points in the complex plane. A circle is fit through

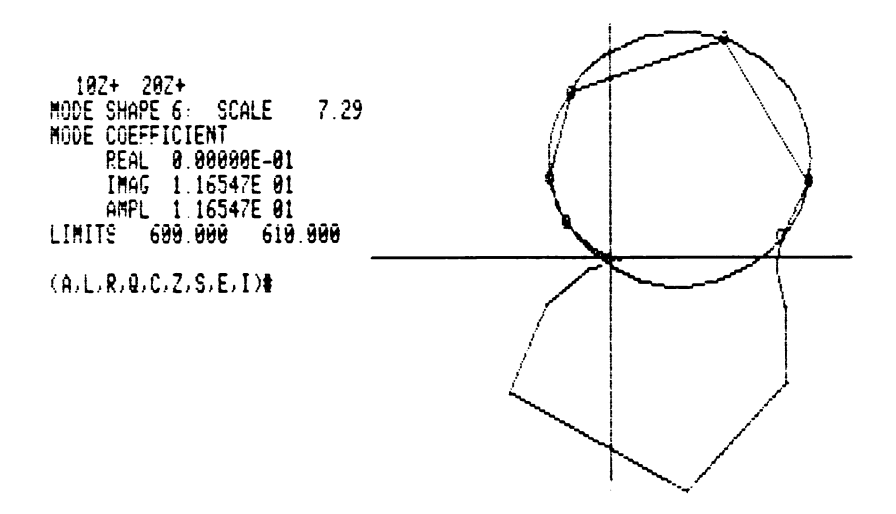
these points using a least squares technique. The size and position of the circle on the complex plane is sufficient information to characterize the motion for a single point on the structure at the natural frequency of interest.

The following procedure was used to calculate mode shapes for the flywheel. The mode shapes were calculated one at a time beginning with the lowest natural frequency. First, a digital cursor was applied to a frequency response function to determine a frequency band which included the peak of interest. The SDOF circle fitting technique was then applied to each of the 48 frequency response functions using the same frequency band. If the circle fit was inadequate, the frequency band was temporarily adjusted to take more or less data from either the higher or lower frequency side of the peak. If necessary, several iterations were done on the frequency band to obtain a good fit. The data was then stored and the next frequency response function was fit with the original frequency band. Figure 3-10 shows a typical circle fit before and after "fine tuning". When all the frequency response functions were fit for the natural frequency, the animated mode shape could be viewed. The procedure was then repeated until all six mode shapes were calculated.

This procedure yields both magnitude and phase. The diameter of the circle is related to the magnitude of the displacement for the particular node at the natural frequency in question, and the position of the circle on the complex plane defines the phase of the displacement relative to the reference coordinate. With this information for each node and the geometric data denoting



a) Original Frequency Band.



b) Limited Frequency Band.

Figure 3-10 Single Degree of Freedom Circle Fits.

their spatial relationship, the mode shape animation is accomplished using linear interpolation between nodes.

The SDOF circle fitting technique is discussed in detail in Reference [2] and [4].

Figure 3-11 shows the mode shape associated with the first natural frequency. It is shown in one extreme position.

3.7 Validity of Modal Data Base

To gain confidence in the results of the modal test, a check of the validity of the modal data base must be performed. This is accomplished by synthesizing an analytical frequency response function from the extracted modal parameters. The synthesized function can then be compared to the measured data.

The synthesized function is constructed with an analytical summation of all the modes extracted. In this case, the frequency response function for the continuous structure is approximated by a summation of 6 modes of vibration. Figure 3-12 shows a synthesized frequency response function superimposed over the actual measured data. The fit is very good, indicating that the modal data base and results obtained from it are reliable.

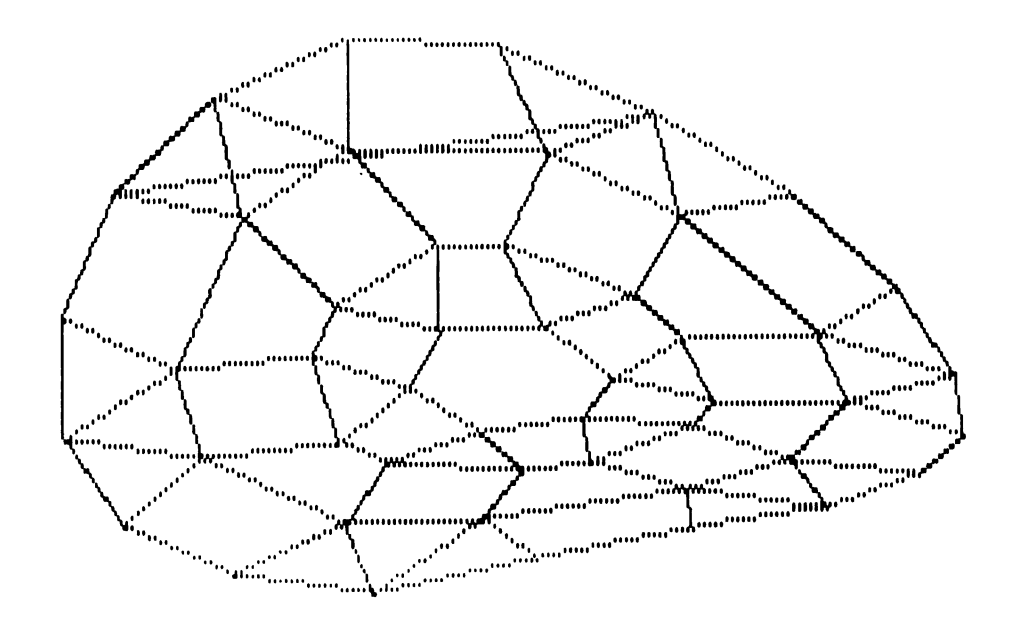


Figure 3-11 Mode Shape at First Natural Frequency (Experimental).

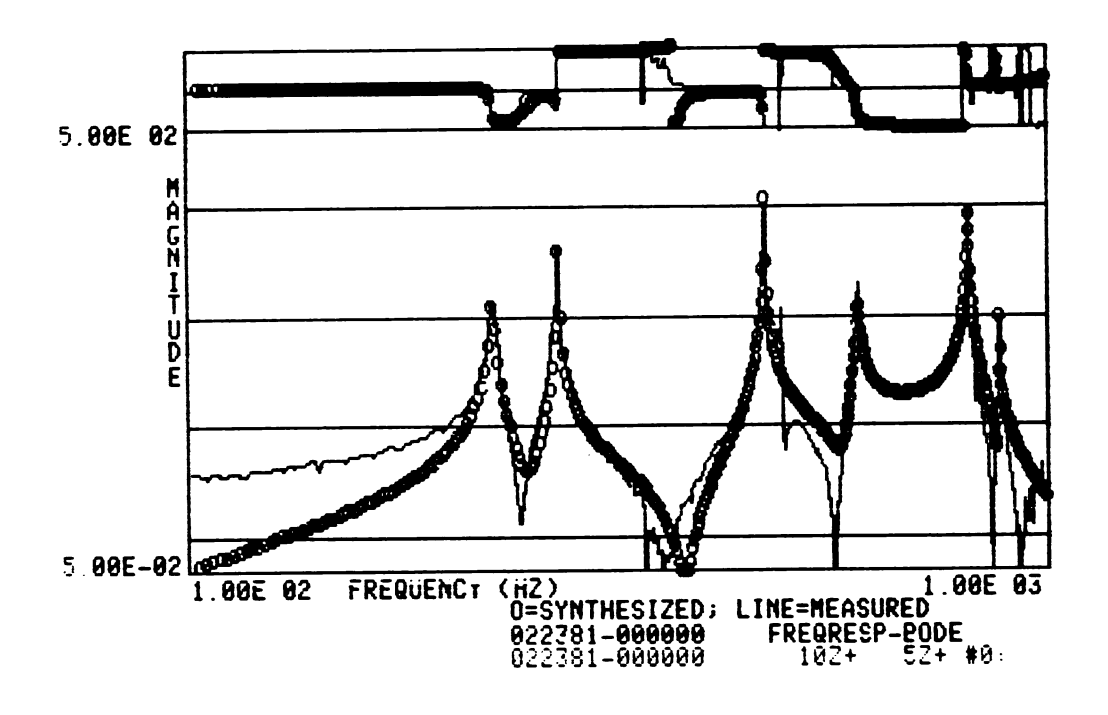


Figure 3-12 Synthesized Frequency Response Function.

ANALYTICAL MODAL ANALYSIS

Analytical methods in structural dynamics have been studied for many years. For example, the transverse vibration of uniform circular plates was a popular topic of concern for scientists and mathematicians in the 18th and 19th centuries. The most notable researcher in this area, Lord Rayleigh, published a comprehensive compilation of the current plate theory in <a href="https://doi.org/10.1007/jhear.1007

Purely analytical methods, however, are not particularly useful for problems with complicated geometry and/or boundary conditions. The advent of modern computing hardware and software now makes it possible to deal with such complex problems in a relatively accurate and efficient manner. This most often entails use of the finite element method.

A common human trait, when presented with a large complex problem, is to deal with only a small part of it at a time. The finite element method involves discretization of a large continuous structure into a number of smaller elements. By formulating the equations governing each element with its individual boundary and loading conditions, the system of equations describing the behavior of the entire structure can be assembled. Assembly and solution of the large system of equations is made possible with

the use of high speed digital computers. Interactive graphics hardware and software simplifies the formulation of the mathematical model, as well as presentation of the results.

This chapter presents a brief background of the finite element method which was used to perform modal analysis on the flywheel.

4.1 Modal Analysis via the Finite Element Method

Many important engineering problems that can be defined by partial differential equations can be solved with the finite element method. This section will be limited to the finite element method as applied to linear free vibration problems, specifically, modal analysis.

The equation of motion for a structural system that is undamped and has no forces applied (free vibration) may be expressed as a set of simultaneous second order linear differential equations. These may be written, in matrix notation, as:

[M]
$$\{\ddot{u}(t)\} + [K] \{u(t)\} = \{0\}$$
 (4-1)

where:

[M] = mass matrix

[K] = stiffness matrix

{u(t)} = acceleration vector

{u(t)} = displacement vector

If the system has m degrees of freedom, then the matrices are m by m and the vectors are m dimensional. In some finite element programs, equation 4-1 is condensed to a more manageable size before the eigenvalues and eigenvectors are extracted. One such reduction procedure will be discussed in Section 4.2. The reduced form of equation 4-1 may be written as:

$$[\hat{M}]$$
 $\{\hat{u}\}$ + $[\hat{K}]$ $\{\hat{u}\}$ = $\{0\}$ (4-2)

The matrices are now n by n (where n<m) and the vectors are n dimensional.

For a linear system, free vibrations will be harmonic of the form:

$$\{\hat{\mathbf{u}}\} = \{\hat{\psi}_i\} \cos \omega_i \mathbf{t} \tag{4-3}$$

where:

 $\{\hat{\psi}_{\hat{1}}\}$ is the eigenvector representing the shape of the ith frequency

 ω_i is the ith natural frequency (rad/time)

t indicates time

Combining equations 4-3 and 4-2 yields:

$$(-\omega_{i}^{2} [\hat{M}] + [\hat{K}]) \{\hat{\psi}_{i}\} = \{0\}$$
 (4-4)

This is an eigenvalue problem with n values of ω_{i}^{2} and n eigenvectors $\{\psi_{i}\}$ which satisfy equation 4-4. The solution of equation 4-4 may be obtained through matrix iteration techniques [7].

4.2 ANSYS

Modal analysis was performed on the flywheel using ANSYS.

ANSYS is a general purpose finite element program developed by
Swanson Analysis Systems Inc. The ANSYS program employs a matrix
reduction technique refered to as dynamic (or kinematic) matrix
condensation. This procedure involves specification of a certain
number of "master" degrees of freedom (MDOF). The mass and
stiffness matricies are then condensed to these n master degrees
of freedom, and the eigenvalue problem is solved. This feature
allows ANSYS to efficiently solve for the response of a very large
structural system. The following discussion deals with the
criterion used to select master degrees of freedom as well as
the process of matrix reduction.

A finite element model is created by defining a number of points (nodes) on a coordinate system. The nodes are then connected to form elements in a manner that closely approximates the actual geometry of the structure. (Modelling will be discussed further in Section 4.3.) The number of degrees of freedom per node is determined by the type of element selected. For instance, a two dimensional plate element has three degrees of freedom per node; rotation about two axes in the plane of the element and translation normal to that plane. A quadrilateral shell element

has six degrees of freedom per node, translations and rotation about all three axes.

The purpose of defining a set of master degrees of freedom is to reduce the complexity of the analysis by including only enough degrees of freedom to characterize the behavior of the system. Selection of master degrees of freedom can be viewed as a further discretization of the model. If dynamic matrix condensation were not used, the problem could be reduced in size by simply modelling with fewer elements. However, this simplification would be at the expense of the accuracy of the modelled stiffness. Reduction of the full displacement stiffness and mass matricies to the master degrees of freedom requires information relating the master degrees of freedom to the removed (or slave) degrees of freedom. Thus, the structure may be modelled with sufficient elements to characterize the stiffness, while dynamic matrix condensation provides efficient solution of the large matrix problem. Successful use of the master degrees of freedom requires that the degrees of freedom associated with the lowest modes of vibration be selected. The following guidelines are suggested by Swanson Analysis Inc. for selecting master degrees of freedom when bending type modes are of primary concern [8]:

- 1. Neglect rotational degrees of freedom.
- 2. Neglect stretching modes.
- The number of master degrees of freedom should be at least twice the number of modes of interest.
- 4. Include master degrees of freedom locations having relatively large mass.

Current versions of ANSYS are capable of automatically selecting any number of master degrees of freedom. The total number of master degrees of freedom must be specified. The user may then specify some master degrees of freedom and allow the program to select the rest or, allow ANSYS to automatically select them all. The program examines all the degrees of freedom sequentially and attempts to retain those corresponding to the lowest modes.

Dynamic matrix condensation is most easily explained by considering the static equation [9]

$$[K] \{u\} = \{F\}$$
 (4-5)

where [K] = total stiffness matrix $\sum_{m=1}^{N} [K_e]$

{u} = displacement vector

{F} = load vector

N = number of elements

 $[K_e]$ = element stiffness matrix

Equation 4-5 may be partitioned into two groups, the master (retained) degrees of freedom, denoted by the subscript "m", and the slave (removed) degrees of freedom, denoted by the subscript "s".

$$\begin{bmatrix} K_{mm} & K_{ms} \\ - - & K_{sm} & K_{ss} \end{bmatrix} \qquad \begin{cases} U_{m} \\ - & K_{sm} & K_{ss} \end{bmatrix} \qquad \begin{cases} V_{m} \\ V_{s} & K_{sm} & K_{ss} \end{cases}$$
 (4-6)

or, expanding: .

$$[K_{mm}] \{U_{m}\} + [K_{ms}] \{U_{s}\} = \{F_{m}\}$$
 (4-7)

$$[K_{sm}] \{U_m\} + [K_{ss}] \{U_s\} = \{F_s\}$$
 (4-8)

Solving equation 4-8 for $\{U_S^{}\}$,

$$\{U_{s}\} = [K_{ss}]^{-1} \{F_{s}\} - [K_{ss}]^{-1} [K_{sm}] \{U_{m}\}$$
 (4-9)

Substituting $\{U_{S}^{}\}$ into equation 4-7:

$$([K_{mm}]-[K_{ms}][K_{ss}]^{-1}[K_{sm}])\{U_{m}\} = (\{F_{m}\}-[K_{ms}][K_{ss}]^{-1}\{F_{s}\})$$
(4-10)

or,

$$[\hat{K}] \{\hat{U}\} = \{\hat{F}\}\$$
 (4-11)

where:

$$[\hat{K}] = [K_{mm}] - [K_{ms}][K_{ss}]^{-1}[K_{sm}]$$
 (4-12)

$$[\hat{F}] = [F_m] - [K_{ms}][K_{ss}]^{-1} \{F_s\}$$
 (4-13)

$$\{\hat{\mathbf{U}}\} = \{\mathbf{U}_{\mathbf{m}}\} \tag{4-14}$$

For modal analysis (equation 4-1) the load vector {F} in equation 4-5 equals zero.

The mass matrix cannot be reduced directly as described above because the condensed matrices would be functions of the time derivatives of displacement and very awkward to implement. Therefore, the program applies the Guyan reduction procedure resulting in the reduced mass matrix:

$$[\hat{M}] = [M_{mm}] - [K_{ms}][K_{ss}]^{-1}[M_{sm}] - [M_{ms}][K_{ss}]^{-1}[K_{sm}]$$

$$+ [K_{ms}][K_{ss}]^{-1}[M_{ss}][K_{ss}]^{-1}[K_{sm}] \qquad (4-15)$$

ANSYS solves the reduced eigenvalue problem (equation 4-4) by applying the Jacobi iteration procedure [1],[7]. The solution consists of m natural frequencies ω_i and m eigenvectors $\{\hat{\psi}_i\}$, each of which represent the mode shape of the structure at the corresponding frequency. Each eigenvector is then normalized such that:

$$\{\hat{\psi}_i\}^T \begin{bmatrix} \hat{\mathsf{M}} \end{bmatrix} \{\hat{\psi}_i\} = 1$$
 (4-16)

The reduced eigenvectors are then expanded to the full set of structure modal displacement degrees of freedom by using equation 4-9 (with $\{F_s\}=\{0\}$). That is:

$$\{\psi_{s}\}_{i} = [K_{ss}]^{-1} [K_{sm}] \{\hat{\psi}\}_{i}$$
 (4-17)

This facilitates display of the structure's mode shapes.

Derivation of element stiffness and mass matrices for a two dimensional plate element is presented in Pages 2.55-2.63 of the ANSYS Theoretical Manual [9].

4.3 Modelling

Finite element models of the flywheel were created with the ANSYS preprocessor, PREP7. PREP7 has sophisticated geometry generation capabilities which facilitate easy creation of complicated geometries. The utility of the preprocessor is significantly enhanced when used on an interactive graphic computer terminal.

Since manufacturer's drawings of the flywheel were unavailable, a full scale drawing was made with dimensions scaled from the flywheel itself. A 60° segment of the drawing, encompassing one of the 6 large circumferential holes, was used as the basis for generation of the geometry. This segment was chosen because the model is symmetric in 60° increments. PREP7 created the five similar segments from the basis segment. Figure 4-1 shows the full element grid.

In this model, two-dimensional triangular and rectangular elements were used (STIF6 and 46). Since, the accuracy of results decreases as the shapes deviate from regular triangles and rectangles [8], the major concern in nodal point location was to maintain regularly shaped polygons. Parallelogram shaped elements were also acceptable because the theory for rectangular elements is based in general on parallelograms.

The model consists of 216 nodes and 234 elements. Several modelling approximations were necessary to keep the model at a

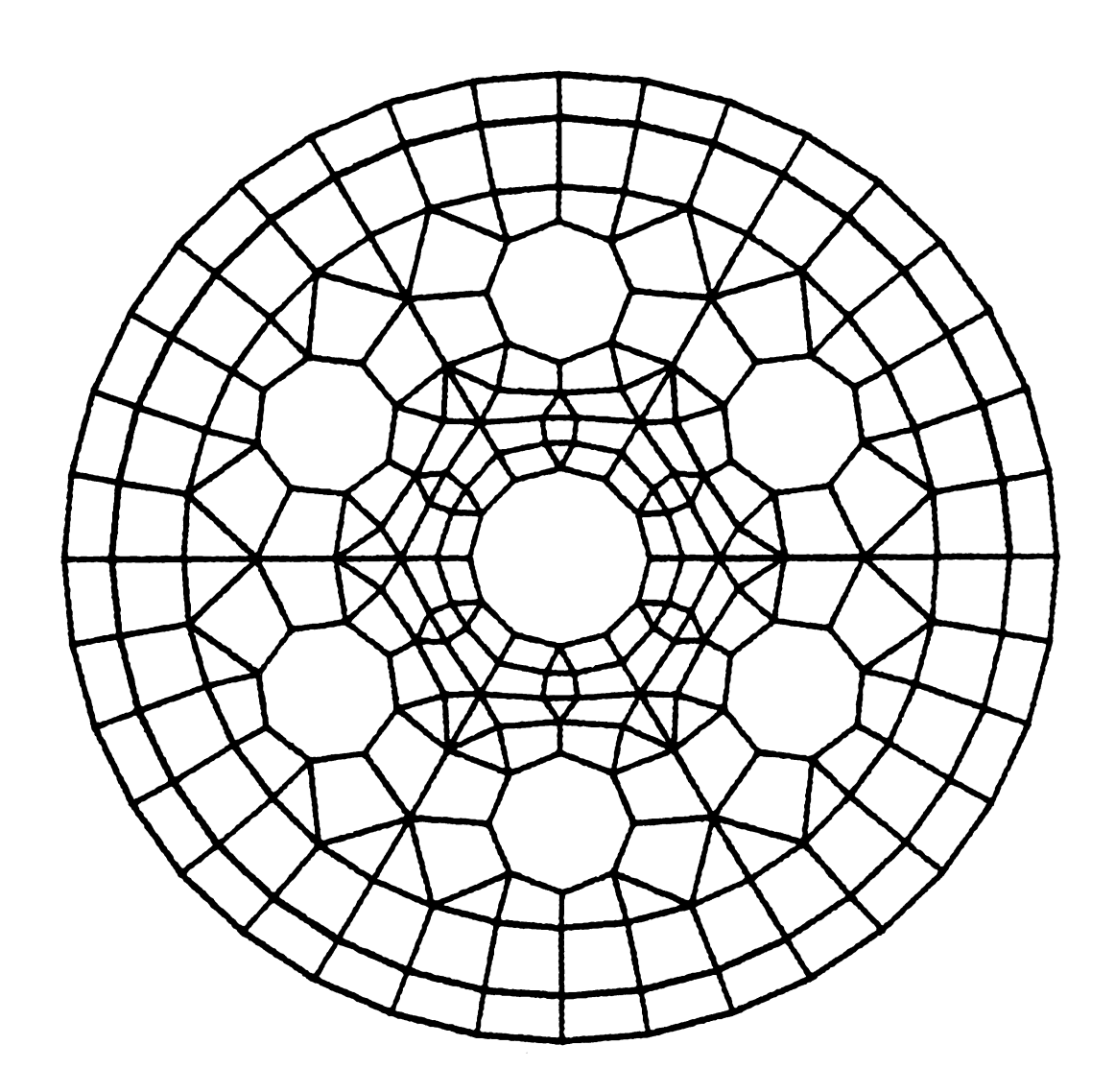


Figure 4-1 Element Mesh.

manageable size. For example, the large circular circumferential holes were approximated by octagons. A mean radius was chosen to smooth the gear teeth on the outer ring. The small interior circumferential "mounting" holes were modelled as rectangles, while several small holes near the outer ring (see Figure 2-1) were not considered at all. The outer gear ring and the interior disk were modelled as one continuous piece, neglecting the welds that actually fasten the two pieces. And the slight curvature of the interior section was initially neglected. Though the size of elements was based on shape considerations, the width of the ring of elements directly interior to the gear ring corresponds approximately to the width of the counterweight on the back of the flywheel. This was convenient for later model modifications to assess the effect of the counterweight. (Section 4.5.)

A caliper micrometer was used to measure thickness of the flywheel. The thickness of the outer most (gear) ring of elements was 0.371 inches, whereas the interior disk thickness was 0.112 inches. Slight variations in thickness were observed, probably due to manufacturing tolerances and/or the effect of sand-blasting. The modulus of elasticity was estimated as 30 $\times 10^6$ psi. Poisson's ratio was estimated as 0.27, and weight density as 0.283 $1b/in^3$.

The flywheel was modelled without external forces and pressures, and no displacements were constrained. However, the element type used (STIF6 and 46) allows input for an elastic foundation on which the elements rest. The modal test which

was described in Chapter 3, revealed rigid body modes in the range 15 to 20 Hz. The value of the foundation stiffness was chosen such that the frequency of the rigid body modes corresponded to those from the modal test. These are well below the first observed bending mode at 227 Hz.

This model was loaded and an initial modal analysis was performed. Figure 4-2 shows the mode shape corresponding to the first natural frequency obtained for this model.

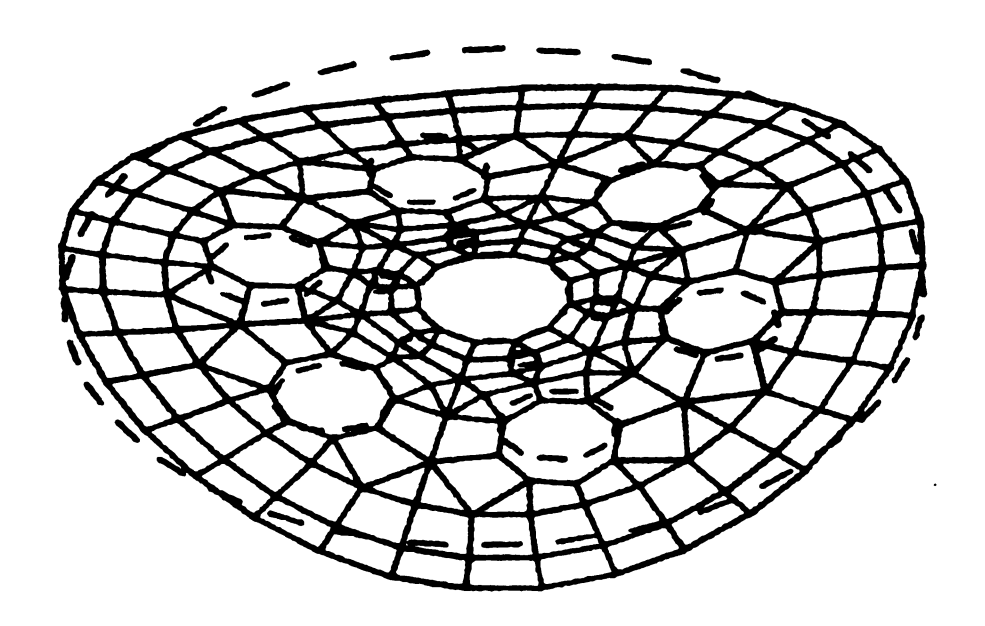


Figure 4-2 Mode Shape at First Natural Frequency. (Finite Element Method).

4.4 Model Verification

A second model, with refined mesh around the outer circumferential holes, was created to determine whether the base model (Figure 4-1) had a sufficient number of elements. Figure 4-3 shows the refined model. This model consists of 288 nodes and 264 elements. Note that the outer circumferential holes were modeled as twelve sided polygons as opposed to octagons used in the base model.

The refined model was loaded into the main program and the modal analysis was performed. The same physical and material properties used in the base model run were applied to the refined model. Also, the same number of master degrees of freedom were used in both analyses.

Table 4.1 summarizes the correlation of the first six natural frequencies between the two models. The table indicates only slight differences between the results for the two models. The base model was, therefore, judged sufficient and all further analyses were based on that geometry.

The fifth and sixth modes in Table 4.1 were found in opposite order in the modal test. That is, the modal test indicated the sixth mode in Table 4.1 occurred at a lower frequency than the fifth. This indicated further model refinement was necessary.

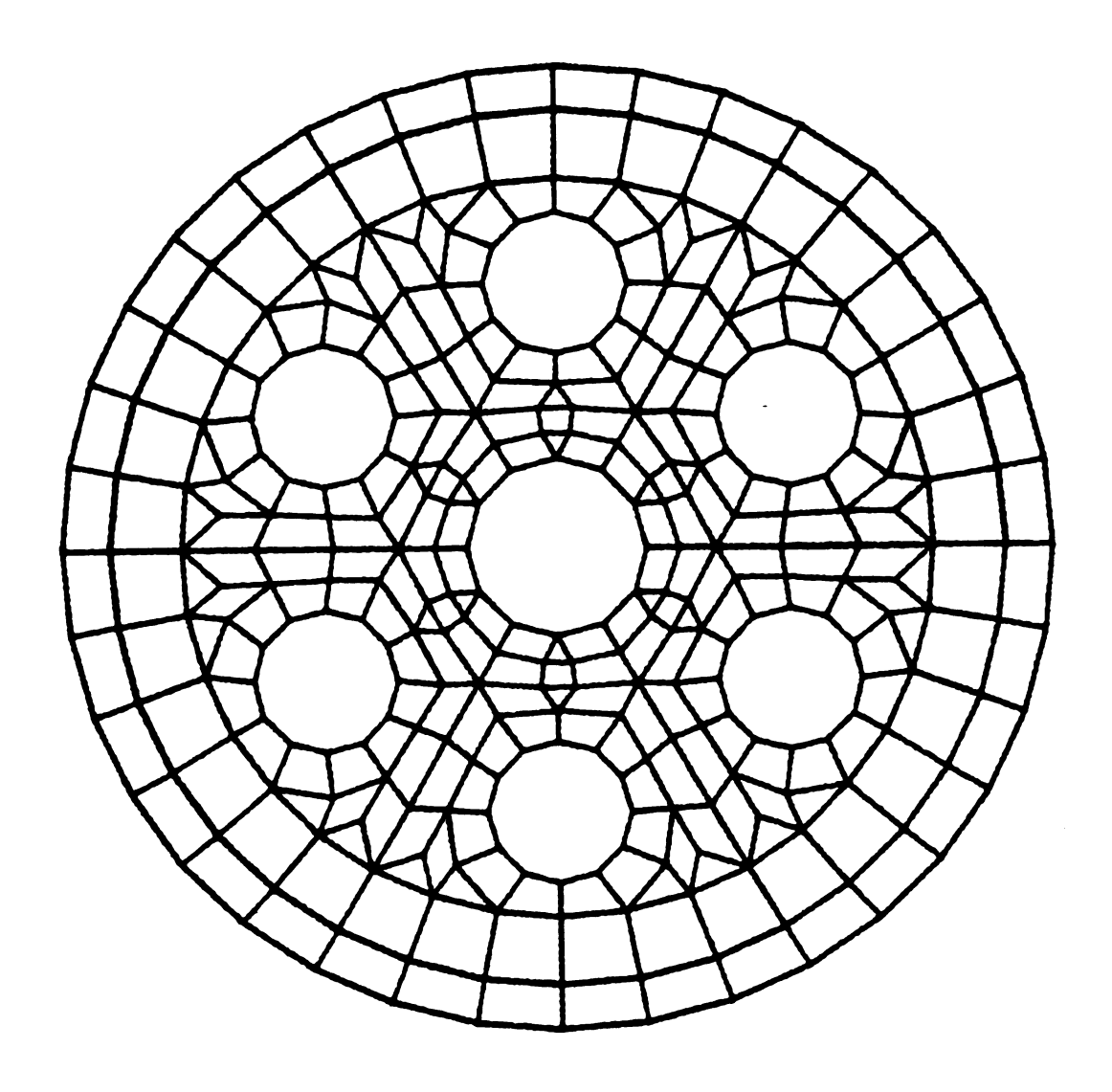


Figure 4-3 Refined Element Mesh.

TABLE 4.1

Effects of the Refined Element Mesh

Natural Frequencies (HZ)

<u>Mode</u>	Base Model	Refined Model
1	221.2	221.0
2	266.0	266.3
3	563.7	562.9
4	612.2	610.0
5	974.7	975.5
6	987.4	986.2

4.5 Analysis of results

Several modal analyses were performed with the base geometry to assess the effects of various modifications of the model. The modal test data were used as criterion to qualify a model change as detrimental or beneficial to the analysis. This section will present the effects of the following variations:

- Inclusion of the counterweight
- Number and method of selection of master degrees of freedom
- Modified material properties

4.5.1 Counterweight

Figure 4-4 shows the base geometry with shading denoting the approximate location of the counterweight. The shaded elements were modified to determine how inclusion of the counterweight

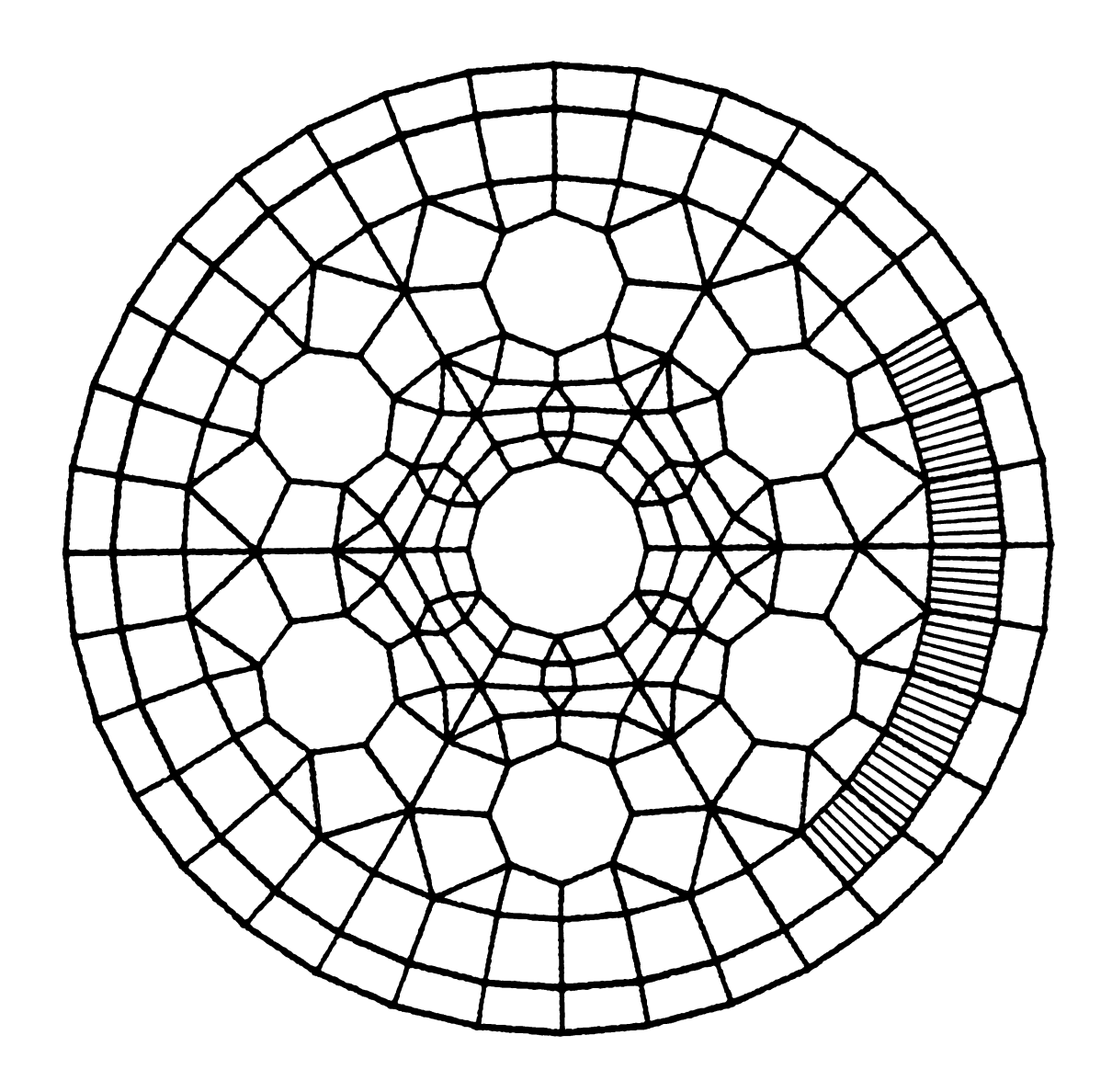


Figure 4-4 Element Mesh with Counterweight Location Denoted by Shading.

effects the dynamics of the base model. First, thickness was added to the shaded elements. This change adds bending stiffness and mass to this section of the model. Second, the density of the shaded elements was adjusted so that they contributed additional mass to the model while leaving the stiffness unchanged. This modification was considered because significant stiffness contribution of the counterweight seemed doubtful. Figure 2-lb indicates that the counterweight itself has 8 holes along its length. This would considerably reduce bending stiffness as compared to a piece with uniform cross section. Also, the counterweight is attached to the flywheel with several small welds. These could not be expected to transmit significant bending moments.

Table 4.2 summarizes the results of the counterweight analysis. The table presents frequency results for (a) the base model (without counterweight), (b) the counterweight modelled with stiffness and mass (thickness adjusted) and (c) the counterweight modelled with adjusted density. The modified thickness model effectively decreased the agreement between the analysis and the experimental results. The modified density model moved the third frequency in the right direction but only by a small amount. The change in frequency was generally small enough to conclude that the counterweight had little effect on the dynamics of the structure. For these reasons, the counterweight was not considered in the remaining analyses.

4.5.2 Master degrees of freedom

The number of master degrees of freedom, and the manner in which they are chosen, have significant effect on the results of the modal analysis. The ANSYS users manual recommends the number of master degrees of freedom be at least twice the number of modes of interest. In this case, the first six bending modes of vibration were desired. However, modal analysis of the base model includes three rigid-body modes (since plate elements allow three degrees of freedom per node), as well as several redundant solutions. Double roots occur due to symmetry of the base model. Modes characterized by nodal diameters (see Figure 4-2) can be expressed in two unique mode shapes. Theoretically, the frequency of the two redundant mode shapes should correspond exactly. But due to the numerical analysis involved in matrix condensation, the frequencies of the double roots tend to deviate progressively with higher modes.

So, in order to obtain the first 6 bending modes, the first 13 modes from ANSYS must be considered. Thus the minimum number of master degrees of freedom for this analysis, based on the recommendation in the User's Manual, is 26. Table 4.3 presents the frequency results for runs with 30, 40, 60, and 80 master degrees of freedom. All other parameters remained constant for these comparison runs. In each case the master degrees of freedom were selected automatically. As expected, the lower frequencies correspond well, and discrepancies increase with the higher modes. Since the PRIME 750 computer was equipped with only one-half megabyte of memory at the time of these runs, the computing

TABLE 4.2
Counterweight Analysis

Natural Frequencies (HZ)

<u>Mode</u>	Base Model	Thickness Adjusted for Counterweight	Density Adjusted for Counterweight
1	221.2	222.8	214.1
2	266.0	277.6	265.1
3	563.7	584.3	562.8
4	612.2	621.3	592.8
5	974.7	982.5	964.2
6	987.4	1032.9	985.2

TABLE 4.3

Effects of the Number of Master Degrees of Freedom

Base Model Natural Frequencies (HZ)

<u>Mode</u>	30 MDOF	40 MDOF	60 MDOF	80 MD0F
1	222.8	221.7	221.2	221.2
2	266.9	266.2	266.0	266.0
3	570.3	565.5	563.7	563.8
4	645.3	623.6	612.2	609.0
5	1016.1	990.3	974.7	973.8
6	1040.6	998.4	987.4	986.2

time increased significantly with the increase in the number of master degrees of freedom. Thus for the remaining analyses, 60 master degrees of freedom were used. This number seemed a good compromise between compute time and accuracy of results.

The method of selection of master degrees of freedom, manual, automatic, or a combination of both, has a more subtle influence on the analysis. A useful technique is to make an initial run with all the master degrees of freedom selected automatically. Then after observing the character of the mode shapes, a second run can be done specifying master degrees of freedom in areas of large or complicated displacements. This procedure was applied throughout the modal analysis of the flywheel. Slight improvement in the agreement between the analysis and the experimental results were usually obtained.

4.5.3 Material property modification

To obtain better correlation with the experimental results the modulus of elasticity of the model was varied. Chapter 2, indicated that the flywheel is apparently made in two separate parts and welded together. The interior disk appears to have been stamped from sheet steel, while the outer gear ring was probably cast. Since the material properties of each of these two parts was unknown, a significant difference in the properties was possible.

Several runs were made successively decreasing the modulus of elasticity of the interior disk while holding the outer gear ring constant at 30×10^6 psi. The experimental results were

used as a goal. Table 4.4 presents the frequency results of the base model and the optimum adjusted model. The modulus of elasticity of the interior disk which provided the best correlation to experimental results was 23.5×10^6 psi. Note that the fifth and sixth modes switched to the order predicted by the modal test. These results are compared to experimental values in Chapter 5.

TABLE 4.4

Effects of Material Property Modification

Natural Frequencies (HZ)

<u>Mode</u>	Base Model	Modified "E" Model
1	221.2	217.8
2	266.0	247.2
3	563.7	514.6
4	612.2	603.4
5	974.7	898.6
6	987.4	891.5

Chapter 5

PRESENTATION OF RESULTS

This chapter presents a comparison of results from the analytical and experimental modal analyses. First, the correlation of mode shapes between the two techniques is presented. Second, a comparison of natural frequencies obtained from the modal test and the best estimate finite element model will be discussed. And, finally, the thesis is summarized in a brief overview.

5.1 Mode Shape Correlation

Figures 5-1 through 5-6 present the mode shapes obtained from the modal test of the flywheel, and Figures 5-7 through 5-12 show the mode shape results from the finite element analysis. The analytically derived mode shapes are displayed with the aid of the ANSYS post-processor POST25, which presents the element mesh in the deformed position while the dashed outline represents the static, undeformed shape. Mode shapes obtained experimentally are shown in one extreme displacement. In these figures, the undeformed shape was omitted for clarity.

Mode shapes for circular disk type structures may be conveniently categorized by identifying nodal diameters and nodal circles. The nodal lines represent points on the structure which

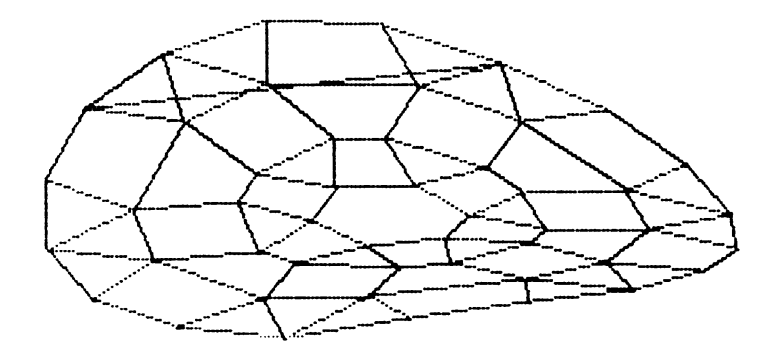


Figure 5-1 First Mode Shape - Experimental.

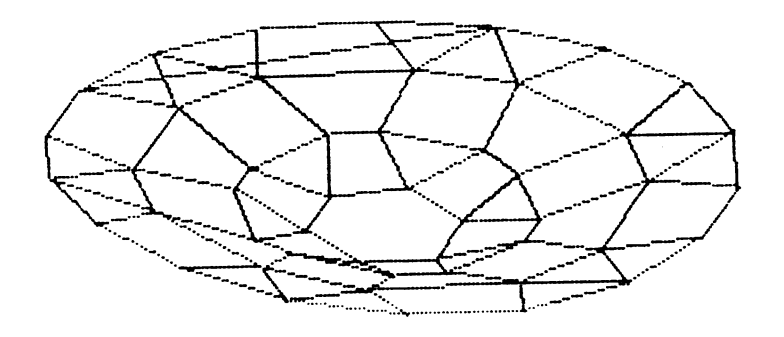


Figure 5-2 Second Mode Shape - Experimental.

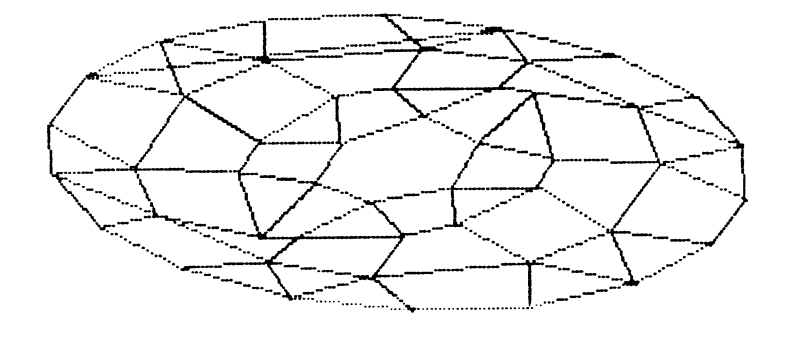


Figure 5-3 Third Mode Shape - Experimental.

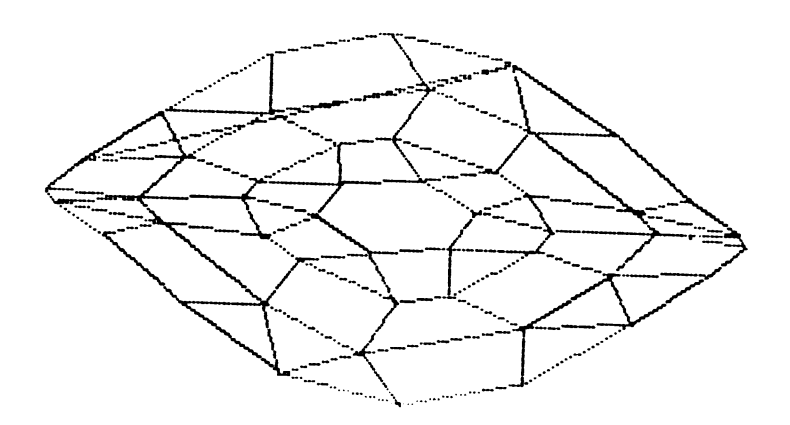


Figure 5-4 Fourth Mode Shape - Experimental.

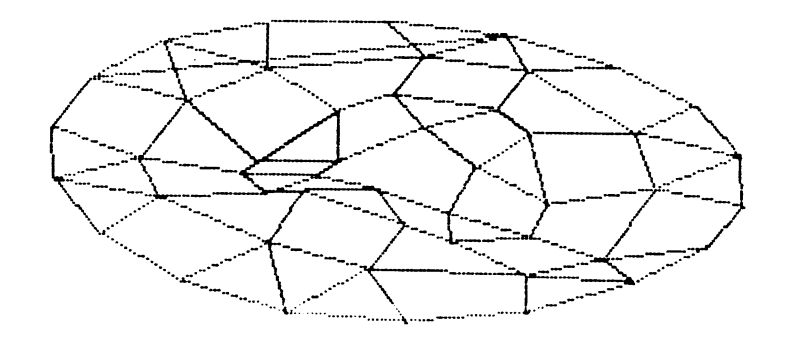


Figure 5-5 Fifth Mode Shape - Experimental.

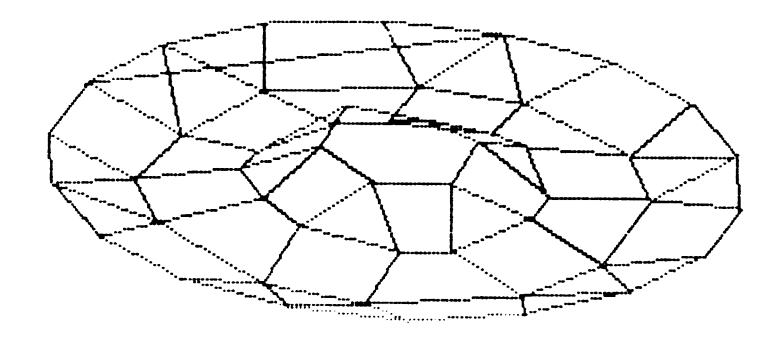


Figure 5-6 Sixth Mode Shape - Experimental.

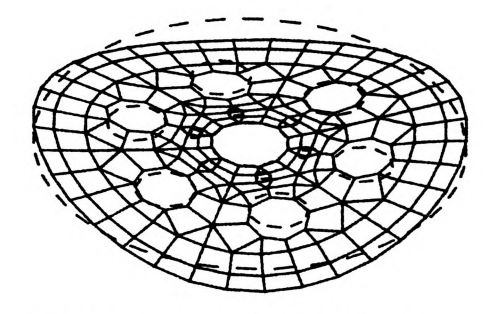


Figure 5-7 First Mode Shape - Finite Element Method.

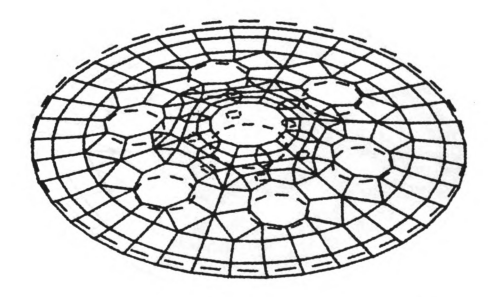


Figure 5-8 Second Mode Shape - Finite Element Method.

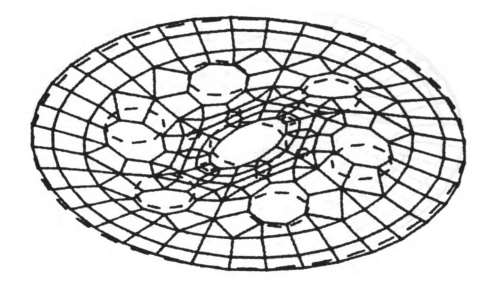


Figure 5-9 Third Mode Shape - Finite Element Method.

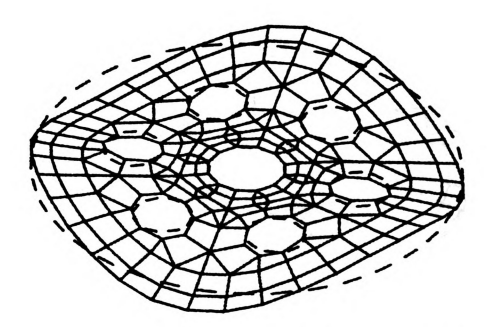


Figure 5-10 Fourth Mode Shape - Finite Element Method.

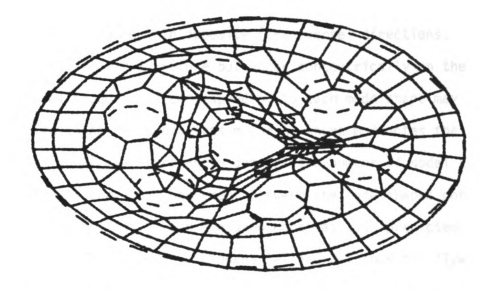


Figure 5-11 Fifth Mode Shape - Finite Element Method.

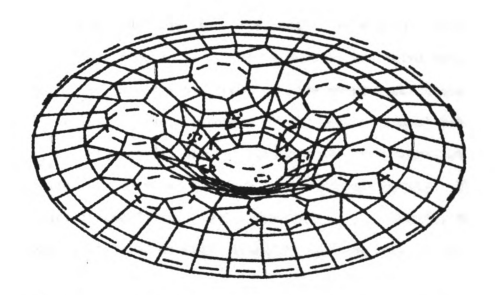


Figure 5-12 Sixth Mode Shape - Finite Element Method.

remain stationary while portions of the structure on either side of the nodal line move in opposite (transverse) directions. Nodal circles are similar in nature but occur concentrically on the disk. The natural frequencies corresponding to each mode shape may be identified using the subscripts m and n; where m denotes the number of nodal diameters and n denotes the number of nodal circles.

There is excellent agreement between the mode shapes obtained from the two methods. Each measured mode was also predicted by ANSYS in the proper order. Figures 5-1 and 5-7 show the flywheel in deformation consisting of two nodal diameters and no nodal circles. These correspond to the first natural frequency, $\omega_{2,0}$. Figures 5-2 and 5-8 show no nodal diameters and no nodal circles. These correspond to the second natural frequency, $\omega_{0,0}$. Figures 5-3 and 5-9 present the third mode, which is characterized by one nodal diameter and one nodal circle. (The nodal circle occurs very close to the outer gear ring.) This shape occurs at the third natural frequency, $\omega_{1,1}$. Figures 5-4 and 5-10 show three nodal diameters and no nodal circles. These correspond to the fourth natural frequency $\omega_{3.0}$. Figures 5-5 and 5-11 present the fifth mode, which is characterized by two nodal diameters and one nodal circle. This shape occurs at the fifth natural frequency $\omega_{2,1}$. Finally, the sixth mode consists of no nodal diameters and one nodal circle. This shape, shown in Figures 5-6 and 5-12, corresponds to the sixth natural frequency, $\omega_{0,1}$.

5.2 Natural Frequency Correlation

A comparison of the natural frequencies obtained from the modal test and the optimum finite element analysis is presented

in Table 4.5. The finite element model used for this analysis employed two different material properties, $E = 30 \times 10^6$ psi for the outer ring and $E = 23.5 \times 10^6$ psi for the inner ring as explained in Chapter 4. The table indicates that the measured and calculated results were always within ten percent.

TABLE 4.5

Analytical and Experimental Results

Natural Frequencies (HZ)				
<u>Mode</u>	Experimental (GENRAD)	Analytical (ANSYS)	Percent Difference	
^ω 2 , 0	227.1	217.8	-4.1	
ω _{0,0}	271.8	247.2	-9.1	
^ω 1.1	470.8	514.6	+9.3	
^ω 3.0	604.4	603.4	~0	
^ω 2,1	812.0	891.5	+9.8	
^ω 0,1	882.8	898.6	+1.8	

5.3 Summary

This thesis has presented an application of two independent methods for performing modal analysis. An experimental technique involving digital signal processing was presented first. Then, a numerical technique using the finite element method was discussed in some detail. The synthesis of these results served as a basis for a discussion of modelling approximations.

Though the results for the flywheel may have little intrinsic value, the comparison of the two independent techniques provided

significant insight in the area of mathematical modelling. The lessons learned from this relatively simple structure can be applied to dynamic analyses of more complicated structural designs.

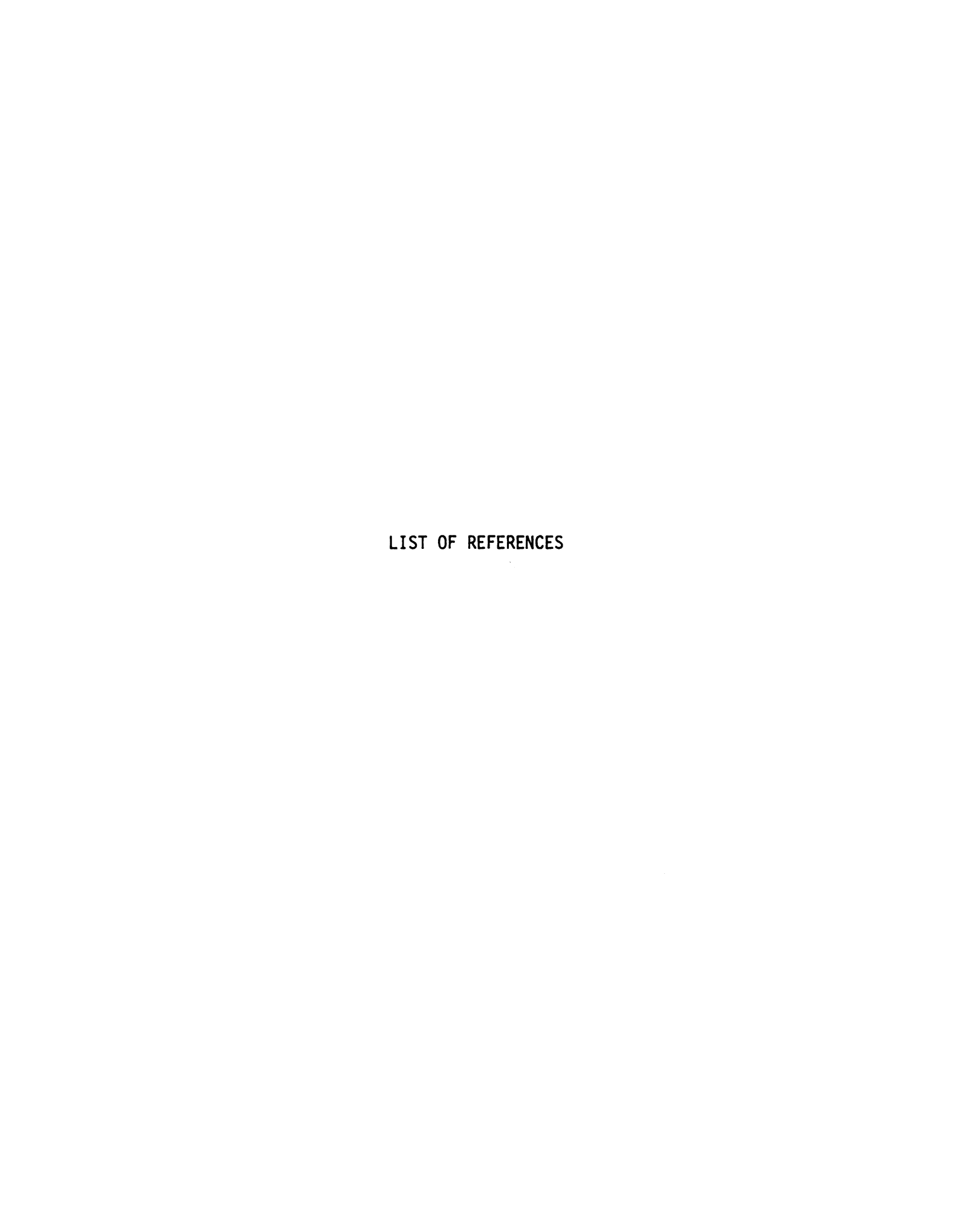
Chapter 6

CONCLUSIONS

The finite element method is widely used because it can handle difficult problems conveniently. However, as this thesis has shown, results from a finite element analysis are only as accurate as the mathematical model.

A possibly significant factor not addressed by this thesis is the effect of residual stresses on the dynamics of the structure. Residual stresses are present, to some extent, in almost all mass produced structural elements. In the flywheel, for example, residual stresses could have been introduced from the stamping process used to manufacture the interior disk, or from the welds which attach it to the outer gear ring. The effects of initial in-plane stress on the free vibration of circular disks are discussed in detail in Reference [10].

Many industries commonly use both numerical and experimental methods for modal analysis. Unfortunately, communication between analysts in these two areas may be limited. This thesis has shown that synthesis of results can be very beneficial. In particular, the merger of these two independent techniques allows the analyst to gain confidence in his mathematical model, thus lending credibility to further more complex analyses.



LIST OF REFERENCES

- 1) Meirovitch, L., "Analytical Methods in Vibrations", Macmillan Co. London, 1967.
- 2) Richardson, M., "Modal Analysis Using Digital Test Systems", Hewlett-Packard Co., Santa Clara, California. Reprinted from Seminar on Understanding Digital Control and Analysis in Vibration Test System.
- 3) Structural Dynamics Research Corporation, "MODAL PLUS Reference Manual", Cincinnati, Ohio.
- 4) Structural Dynamics Research Corporation, "Advanced Trouble-shooting Seminar", Volume 1, Cincinnati, Ohio, 1980.
- 5) Levy, E.C., "Complex Curve Fitting", IRE Trans., AC. 4, 1959.
- 6) Rayleigh, J.W.S., "Theory of Sound", Dover Press, New York, 1945.
- 7) Wilkinson, J.H., "The Algebraic Eigenvalue Problem", Oxford University Press, 1965.
- 8) Swanson Analysis Systems Inc., "ANSYS User's Manual", Houston, Pennsylvania.
- 9) Swanson Analysis Systems Inc., "ANSYS Theoretical Manual", Houston, Pennsylvania.
- 10) Mote, C.D., "Free Vibration of Initially Stressed Circular Disks", ASME Trans., Series B, Vol. 87, 1965.
- 11) Rizai, H.M.N., "The Impact of Modal Analysis on the Engineering Curriculum", M.S. Thesis, Michigan State University, 1980.

